Interface and bulk properties of Fe/Mn sandwich structures

E. C. Passamani,[1,2] B. Croonenborghs,[1] B. Degroote,[1] and A. Vantomme[1]
[1]*Instituut voor Kern-en Stralingsfysica, Katholieke Universiteit Leuven, B-3101 Leuven, Belgium*
[2]*Departamento de Física, Universidade Federal do Espírito Santo, Vitória, 29060-900, ES, Brazil*
(Received 23 September 2002; revised manuscript received 6 March 2003; published 30 May 2003)

Structural and magnetic properties of Fe(5 nm)/Mn(t_{Mn})/Fe(5 nm) (t_{Mn} from 0.5 to 3.0 nm) sandwich structures, grown by molecular-beam epitaxy between 50 °C and 150 °C, were investigated using reflection high-energy electron diffraction (RHEED), x-ray-diffraction, Mössbauer spectroscopy, and magnetization measurements. Epitaxial bct-Mn structures only form for $t_{Mn}<1$ nm, independently of the growth temperature. Room-temperature conversion electron Mössbauer spectra are composed of two magnetic components with in-plane magnetic moments. The first subspectrum has hyperfine parameters close to α-Fe and is therefore associated with Fe atoms far from the interface regions. The second component, fitted with a hyperfine field (hf) distribution, has an isomer-shift value similar to α-Fe and a maximum in the distribution curve at about 31 T. This subspectrum is related to the Fe atoms close to the Mn layer (interface regions). Low-field components in the hf distribution curves indicate the presence of Fe atoms or/and Fe clusters in the Mn spacers. An Fe-Mn alloy was observed for the samples grown for temperatures higher than or equal to 50 °C and where the RHEED patterns show the presence of the α-Mn phase. Magnetization data show that the Fe layers are ferromagnetically coupled for all trilayers prepared at substrate temperatures lower than 150 °C. A noncollinear coupling was found for the trilayer with Mn thickness of 1 nm and grown at 150 °C.

DOI: 10.1103/PhysRevB.67.174424 PACS number(s): 75.70.Cn, 68.35.Ct, 76.60.Es, 75.30.Gw

I. INTRODUCTION

Interlayer coupling between magnetic layers separated by a metallic[1] spacer layer oscillates periodically from ferromagnetic (FM) to antiferromagnetic (AFM) as the thickness of the spacer layers changes. Besides these well-defined collinear magnetic states between the magnetic layers, a possibility for 90° magnetic coupling has also been reported for epitaxial trilayers that have the compositions Fe/Cr/Fe,[2] Fe/(Al, Cu)/Fe,[3] Fe/(Cu)Fe,[4] etc. Only recently arbitrary noncollinear coupling angles were found in Fe/Mn/Fe (Ref. 5) and FeCo/Mn/Fe/Co (Ref. 6) trilayer sandwiches. Extensive research has been done to understand possible coupling mechanisms. In general, for paramagnetic or diamagnetic spacers, the coupling mechanism can be described by using an intrinsic quantum well picture, where the coupling is determined by the Fermi-surface properties of the spacer layer and the reflection amplitudes for electrons scattering at the interfaces between the spacer layer and the FM layer.[7] To explain biquadratic coupling several extrinsic mechanisms are suggested by Demokritov *et al.*[8] However, in the case of AFM spacers, such as Cr and Mn, the spacer layer is not passive, as for nonmagnetic materials. The proximity magnetism model[9] is a phenomenological model for the description of exchange coupling across these kinds of AFM materials including thickness fluctuations due to interface roughness. Within this model the spacer layer magnetic structure is an helicoidal antiferromagnet, and the coupling originates from the direct *d-d* exchange interaction at the Fe-Mn interfaces and propagates through the magnetic ordering of the spacer layer via short-range exchange interaction. Also for sandwich systems, interface effects have been extensively studied in order to understand the coupling mechanism[10] as well as specific interface-related phenomena, such as spin reorientation,[11] the spin-polarization effect,[12] etc.

Fe/Mn trilayers may potentially elicit a similar interest as Fe/Cr, based on the fact that both Cr and Mn are AFM materials. However, in contrast to all other 3*d* elements, which form fcc or bcc crystalline structures, bulk Mn possesses a very complex cubic lattice structure with 58 atoms per unit cell (α-Mn). On the other hand, fcc- and bcc-Mn phases can be formed at high temperatures.[13] Two methods have been reported for the growth of these Mn phases as a metastable state. The first one is by alloying and extrapolating the lattice constant to a zero impurity concentration.[14] The second method is by epitaxial growth on a suitable substrate. Recently, experimental[15,16] and theoretical[17] studies have been reported regarding Mn grown on cubic (001) substrates such as Fe and Ag. The results indicate that the Mn crystalline structures were slightly distorted fcc or bcc phases, called fct (face-centered tetragonal) or bct (body-centered tetragonal), respectively. Qiu *et al.*[17] have shown that the total free energy as a function of the c/a lattice parameter presents two minima, associated with the fct- and the bct-Mn phases, respectively. Thus, choosing a suitable substrate, bct- or fct-Mn layers can be prepared by molecular-beam epitaxy (MBE).

Theoretical calculations suggest that Mn atoms at the interface couple antiferromagnetically with Fe atoms.[18] This is in agreement with the experimental results obtained by Roth *et al.*[19] on bare Mn thin films grown epitaxially on Fe (001) whiskers. They found that the magnetization of the first Mn monolayer is collinear (antiparallel) with the Fe magnetization. Due to this coupling we expect a distinct magnetic hyperfine field (B_{hf}) for Fe atoms at the interface. We can obtain microscopic information about the interfaces by depositing ^{57}Fe selectively at the interface and measuring the hyperfine parameters with Mössbauer spectroscopy (MS).

MS directly probes the density of *s* electrons [isomer shift (IS)] and B_{hf} at the ^{57}Fe nucleus.

Using MS in combination with x-ray diffraction, reflection high-energy electron diffraction (RHEED), and vibrating-sample magnetization, we have investigated structural and magnetic properties of Fe/Mn bi- and trilayers grown on MgO(001) by MBE, for different growth temperatures.

II. EXPERIMENT

The Fe/Mn sandwiches were grown on polished MgO(001) substrates in an MBE system with a base pressure of 6×10^{-11} mbar. Prior to deposition of the layers, the MgO(001) substrates were cleaned with isopropanol followed by an N_2 gas flow. Subsequently, they were introduced in a high-vacuum annealing chamber and kept at 600 °C for one hour, in a vacuum greater than 1×10^{-8} mbar. The films were deposited using three different substrate temperatures (T_S): 50 °C, 100 °C, and 150 °C, with the samples rotating during deposition to ensure lateral uniformity of the films. The ^{nat}Fe (natural Fe, containing ~2% of ^{57}Fe) layers were deposited using an *e*-gun source with flux feedback control, whereas ^{57}Fe (95% enriched) and Mn (99.999%) were evaporated from temperature-stabilized effusion cells. Quartz-crystal monitors, calibrated by Rutherford backscattering experiments, controlled all nominal layer thicknesses. An 8-nm amorphous Si (*a*-Si) capping layer was used to prevent oxidation of the top Fe layer. This Si layer was deposited at temperatures lower than or equal to 10 °C to avoid interdiffusion between Si and the top Fe layer. No Fe-Si phase was observed by any of the characterization techniques that were used, which ensures us that the Si capping layer did not affect our results. The deposition rates of ^{nat}Fe, ^{57}Fe, and Mn were 0.16, 0.07, and 0.04 Å/s, respectively, and the pressure during the deposition was equal to or greater than 1×10^{-10} mbar. The final nominal composition of our sandwich structures was as follows: ⟨MgO⟩/Fe(4 nm)/^{57}Fe(1 nm)/Mn(0.5–3.0 nm)/^{57}Fe(1 nm)/Fe(4 nm)/*a*-Si(8 nm) for several trilayers and ⟨MgO⟩/Fe(4 nm)/^{57}Fe(1 nm)/Mn(0.5 nm)/*a*-Si(8 nm) for one bilayer.

Nominal Mn thicknesses of 0.5–3.0 nm were chosen both to cover the Mn crystalline transition as reported in the literature,[15] as well as to fit the range where the magnetic coupling between the Fe layers changes from FM to noncollinear coupling.[5] The ^{57}Fe layer was chosen to be 1 nm out of 5-nm total Fe thickness in order to have a sufficient count rate during MS and to minimize the effect of the ^{57}Fe that is contained in the 4 nm of ^{nat}Fe.

In situ RHEED analysis was performed using 10-keV electrons incident at an angle of 3° with respect to the film plane. X-ray diffraction, conversion electron Mössbauer spectroscopy (CEMS), and magnetization measurements were performed *ex situ*. X-ray measurements, using Cu K_α radiation, were done in the low angle geometry (2θ=0.5° to 7.0°) to determine the artificial periodic structure and at high angles in order to characterize the crystallographic properties of the layers. Room-temperature (RT) CEM spectra were obtained with a 25-mCi ^{57}Co(Rh) source in a conventional CEMS chamber, using a mixture of He (96%) and CH_4 (4%). The acquired spectra were fitted using a method for a hyperfine magnetic-field distribution (hf) superimposed with one crystalline sextet site. For films, where the α-Mn phase is present, a doublet has been added as well. A linear correlation between hyperfine magnetic field (B_{hf}) and IS was assumed to take the asymmetry of the magnetic sextet into account. The IS values are given relative to α-Fe at RT.

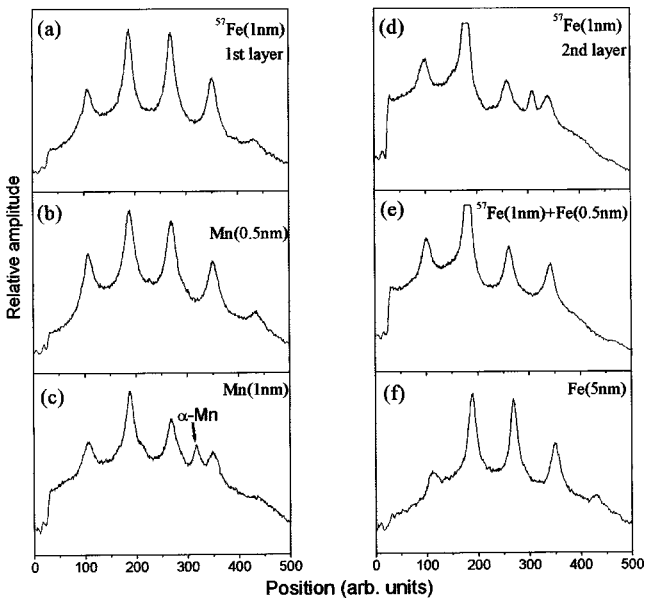

FIG. 1. RHEED diffraction profiles of the ⟨MgO⟩/Fe(5 nm)/Mn(1 nm)/Fe(5 nm) sandwich grown at 150 °C. The RHEED patterns were obtained for different thicknesses of Fe and Mn during the growth process, as indicated in the figure.

Magnetization measurements were done in a commercial Oxford vibrating-sample magnetometer. The measurements cover the temperature range of 10–300 K with magnetic fields applied both in the film plane direction (easy and hard directions of Fe layers) and in the out-of-plane geometry. The maximum applied field value used in this work was 0.5 T, which is sufficient to reach saturation of the magnetization direction, for the in-plane geometry.

III. RESULTS AND DISCUSSION

A. Structural characterization

The RHEED pattern of the first 5-nm Fe layer (^{nat}Fe + ^{57}Fe) deposited on MgO(001) consists of intense streaks corresponding to bcc Fe [see Fig. 1(a)]. However, it is known that the lattice misfit between Fe and MgO is about −3.7% (45° azimuthal rotation of the lattice), which means that the first Fe layer might be elastically strained, as measured by Moons *et al.*[20]

The RHEED pattern of the Mn layer depends on its thickness (t_{Mn}). For $t_{Mn}\leqslant0.5$ nm, they indicate that the Mn layer grows epitaxially on the first Fe layer, with the Mn in-plane

lattice parameter matching with that of bcc Fe.[21] However, the width of the streaks increases, which means that the Mn film is slightly more distorted than the Fe film [compare Figs. 1(a) and 1(b)]. For increasing t_{Mn}, the width of the streaks increases (for $t_{Mn}=1$ nm the width is 6% more than for $t_{Mn}=0.5$ nm, estimated from the RHEED peak at position 270 on the x axis). In addition, spots appear superimposed on the streaks (not visible on the RHEED profile), which indicates that the incident electron beam transmits through blocks or islands nucleated on a flat surface. Henry *et al.*[22] observed similar RHEED spots for Mn/Co multilayers. This suggests a mixture of two- (2D) and three-dimensional (3D) growth modes for Mn layers with a thickness greater than 0.5 nm on Fe, rather than pure layer-by-layer growth.

For $t_{Mn}=1$ nm, an additional streak is clearly visible in the RHEED pattern [see arrow in Fig. 1(c)]. For $t_{Mn}>1$ nm (not shown), a new set of streaks appears, which is less diffuse and has a smaller separation in reciprocal space. This indicates that the corresponding Mn structure has a larger lattice parameter compared to 0.5 nm of Mn. We attribute this new set of streaks to the α-Mn phase, in agreement with the results of Henry *et al.*[22] and Grigorov *et al.*[23] It should be noted that in our films the bct-Mn phase has a maximal thickness of about 1.0 nm, independently of growth temperature. The gradual increase of the width of the bct streaks [Figs. 1(b) and 1(c)] indicates that the structural change from the bct to α Mn may be related to an increasing lattice distortion.

The second Fe layer grows epitaxially on the Mn layer, when $t_{Mn}\leqslant 0.5$ nm. For $t_{Mn}\geqslant 1$ nm, the RHEED pattern of the first Fe monolayers (second layer) has the same features as the 1-nm Mn pattern [Fig. 1(d)]. Only after 1.5 nm of Fe [^{57}Fe(1 nm)+^{nat}Fe(0.5 nm)] are the bcc-Fe streaks visible again and slightly shifted, indicative of the fact that the top Fe layer is relaxed [Fig. 1(e)]. Their intensities get stronger and less diffuse as the thickness of Fe increases. This means that only at an Fe thickness of 1.5 nm (above the Mn layer) does the transmission through Fe islands case (Fe keeps its bcc structure as observed with RHEED and CEMS). Finally, the RHEED patterns of Si capping layers do not show any streaks, but only a diffuse halo, which confirms the amorphous nature of the Si layers. From these RHEED results, we conclude that for future analyses one has to take into account that roughness plays an important role at the Mn/Fe interface, for $t_{Mn}\geqslant 0.5$ nm.

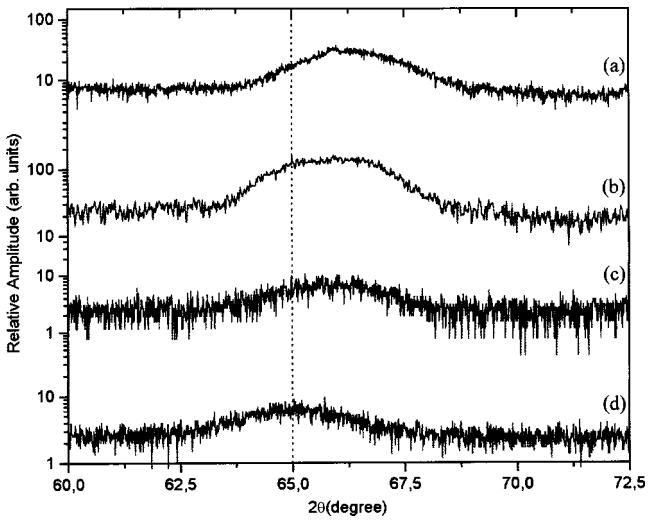

FIG. 2. High angle x-ray-diffraction patterns of the Fe(5 nm)/Mn(0.5 nm) sandwiches prepared at 50 °C [(a) bilayer and (b) trilayer], 100 °C [(c) trilayer], and 150 °C [(d) trilayer].

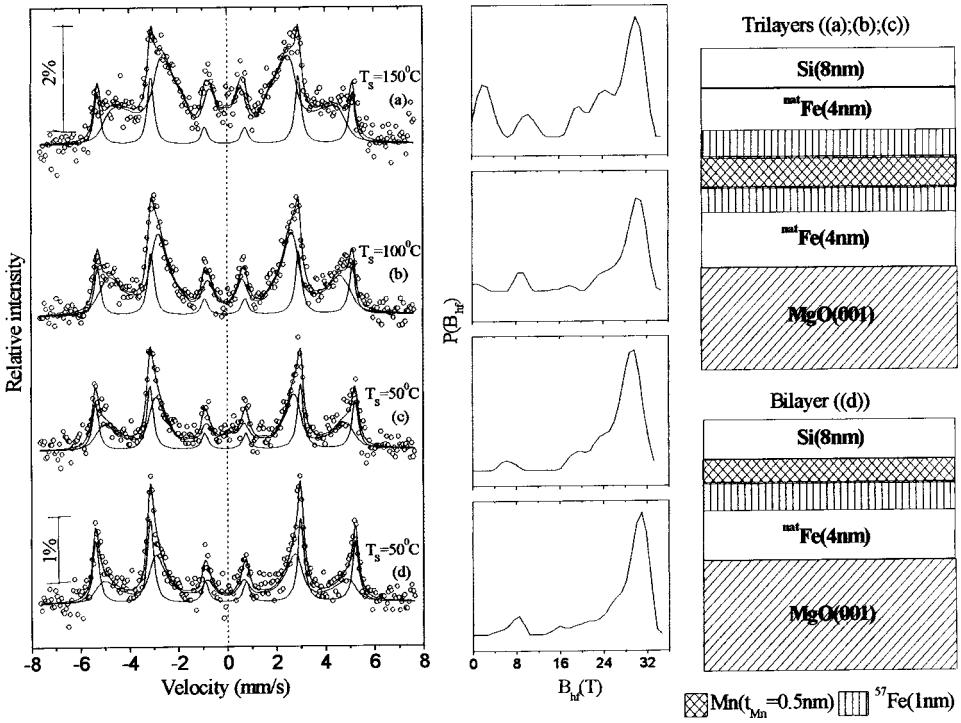

FIG. 3. RT CEM spectra of the Fe(5 nm)/Mn(0.5 nm) bilayer and Fe(5 nm)/Mn(0.5 nm)/Fe(5 nm) trilayers prepared at $T_S=50$ °C, 100 °C, and 150 °C. The points are experimental data, while the full lines correspond to the subspectra and the total fit. On the right side of this figure the B_{hf} distribution curves associated with the interface component are plotted.

Reflectivity measurements, not shown, exhibit well-pronounced oscillations superimposed on an exponential decay for all films, indicating the artificial modulation of the samples. High angle specular x-ray-diffraction patterns of Fe(5 nm)/Mn(0.5 nm) sandwiches (bi- and trilayers) prepared at different T_S are shown in Fig. 2. The dashed line at 65.1° is a reference for the (002) bulk Fe peak. For all samples, only one very broad Bragg peak at approximately 67° can be observed in this angular region. Using the Scherrer formula, the grain size related to the (002) plane is estimated to match the Fe thickness (about 5 nm). This broad peak shifts to lower angular positions with increasing growth temperatures, reaching the bulk (002) Fe angular position for films prepared at 150 °C. Therefore, the peak shift can be understood as a crystalline relaxation process of bcc-Fe layers grown at 150 °C. Moreover, the patterns indicate that the diffraction intensity decreases with increasing growth temperature. This effect may be associated with increasing disorder of the bcc/(bct) phases, or with an increasing interface roughness (lattice distortion) and is further explored using CEMS in the next paragraph. α-Mn reflection lines can only be resolved from the noise for $t_{\mathrm{Mn}} > 1.5$ nm.

B. Magnetic properties

Figure 3 shows the CEM spectra obtained at RT for Fe/Mn sandwiches (bi- and trilayers) prepared at different T_S, but with the same Mn thickness of 0.5 nm. As can be seen from this figure, the spectra are composed of magnetic subspectra only. The fits were performed with two magnetic components. The first one is a sextet that has hyperfine parameters close to the bulk α-Fe phase (IS$=0.01(2)$ mm/s and $B_{\mathrm{hf}}=33$ T), while the second component consists of a hf distribution.

The hf distribution curves (shown at the right-hand side of the Mössbauer spectra of Fig. 3) all have a main peak at about 31 T, and a tail at low-field values, suggesting discrete values of approximately 8, 20, and 24 T. This set of peaks is best resolved in the hf distribution curve of the film prepared at $T_S = 150$ °C. It is important to emphasize that the distribution component is also present in the case of Fe/Mn bilayers grown at 50 °C, showing that the reduction of B_{hf} is due to the presence of Mn atoms, and not solely related to the growth temperature. Wu and Freeman[18] reported that Fe atoms at the interface exhibit a reduction of their magnetic moments due to the influence of the Mn atoms in the Fe neighborhood. This reduction results in a decrease of the effective magnetic hyperfine field ($B_{\mathrm{hf}}^{\mathrm{eff}}$) values at the ^{57}Fe sites, which, in principle, can be described as the sum of two terms: $B_{\mathrm{hf}}^{\mathrm{core}} + B_{\mathrm{hf}}^{\mathrm{CEP}}$ (additional orbital and spin-dipolar contributions are also present, but do not change with the presence of Mn). The first ($B_{\mathrm{hf}}^{\mathrm{core}}$) contribution is mainly due to the Fe magnetic moment, while the second term ($B_{\mathrm{hf}}^{\mathrm{CEP}}$) takes into account the conduction-electron polarization (CEP) due to the presence of Mn atoms and/or to the reduced number of Fe nearest neighbors at the interface. Thus, for a flat interface one would expect that a CEM spectrum should be basically composed of (i) a ^{57}Fe/Mn ideal interface and (ii) bulk-Fe contributions. For a rough interface, however, there are several nonequivalent configurations for ^{57}Fe atoms, i.e., at the corner, step edges or at flat regions, resulting in a broad range of hf values due to the varying CEP effect. There is also a possibility for a disordered alloy formation between the atoms located at the interfaces, resulting in a distribution (magnetic or electric) instead of well-defined Fe sites.

From the hf distribution curves, it can be derived that (i) the IS in the high-field region (larger than 24 T) is close to the IS of the bulk component sextet and (ii) the peak at about 8 T has an IS value of -0.06 mm/s, an indication that this contribution (8%–9% for bi- and trilayers, respectively) is associated with ^{57}Fe atoms (or small Fe clusters) in the Mn layer and/or is due to a larger number of Mn atoms in the lower ^{57}Fe layer. This phenomenon, as well as the fine structure of the hf distribution curves, is discussed below.

The orientation of the Fe magnetic moments was calculated from the ratio of the respective line intensities given by $3{:}x{:}1{:}1{:}x{:}3$ with $x = 4\sin^2(\theta)/[1+\cos^2(\theta)]$, θ being the angle between the incident γ ray and the direction of the magnetization. Since the incident photon direction is along the sample surface normal one should observe 3:4:1:1:4:3 for in-plane magnetization and out-of-plane results in 3:0:1:1:0:3. In our sandwiches, the relative line intensities from the two subspectra indicate that the magnetization of the Fe layers at RT is in the film plane in both cases. From to the results reported above, we conclude that both magnetic components have in-plane magnetization and the first sextet component corresponds to Fe atoms far from the interface (i.e., Fe with only Fe nearest neighbors—bulk Fe), while the distribution component is due to the Fe atoms close to the interface, i.e., the varying number of Mn nearest neighbors is reflected in the hyperfine parameters.

First, the fraction of Fe atoms at the interface region is discussed. Assuming all $^{\mathrm{nat}}$Fe (4 nm in each Fe layer) is a pure α-Fe phase, the fraction of the first sextet component is a measure for the ''unaffected'' part in the ^{57}Fe layer at the interface, after subtracting the $^{\mathrm{nat}}$Fe contribution (2.2% of ^{57}Fe). From this fraction we can calculate the corresponding α-Fe thickness. For the films prepared at 50 °C, the ''unaffected'' Fe thickness is different for the trilayer [(0.56/2) nm $=0.28$ nm] and the bilayer (0.39 nm), which indicates that both interfaces [Mn on Fe (lower) and Fe on Mn (upper)] in the trilayer system are not equivalent to one another. This observation suggests that the lower interface seems to be flatter on an atomic scale (consistency with RHEED observations) and/or shows less ''interdiffusion'' than the upper interface. This difference between lower and upper interfaces is similar to previous observations for Fe/Cr,[10,24,25] Fe/V (Ref. 26) multilayers and others systems.[27] Two models have been applied to describe this effect for nanostructured systems. The first model is based on the binding energies between the substrate and adatom material, which, as a first approximation, is assumed to be proportional to the melting points of the solids. In the case of the Fe/Mn system, the melting point of Mn (1517 K) is lower than that of Fe (1808 K), and therefore, one can expect extensive intermixing for the Fe-on-Mn (upper) interface, but a negligible alloying effect for the Mn-on-Fe (lower) interface. In general, our results fit with the behavior expected by these thermodynamic

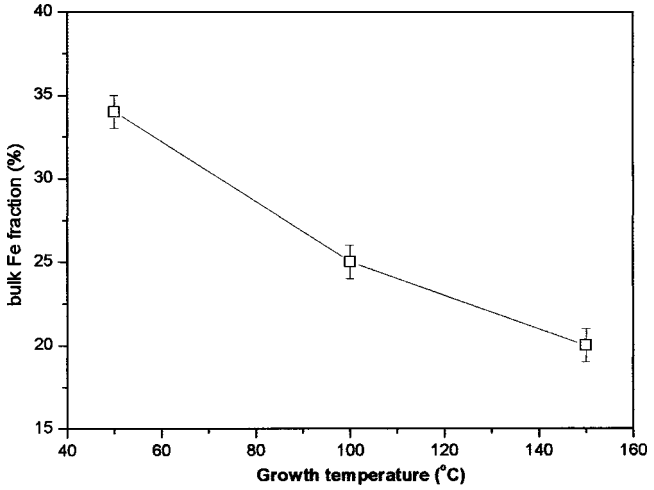

FIG. 4. Fraction of the Fe atoms in the ^{57}Fe layers having bulk Fe properties, as a function of the growth temperature for the trilayers with $t_{Mn}=0.5$ nm. The line connecting the points is only to guide the eyes.

considerations, i.e., the upper interface has a larger mixed fraction than the lower interface if we assume that in bi- and trilayers the lower interfaces are equivalent. On the one hand, the peaks in the hf distribution curves at 8, 20, and 24 T, which have roughly the same fractions (8%–9%, 11%–13%, and 16%–19% of the total distribution component, respectively) for bi- and trilayers prepared at 50 °C, suggest that ^{57}Fe atoms from the lower slabs diffuse into the Mn layers, or a large number of Mn move down to the lower ^{57}Fe slabs. On the other hand, based only on the above-mentioned thermodynamic predictions (first model), a negligible amount of Mn atoms would be expected to diffuse to the lower ^{57}Fe slabs. However, the hf distribution curves show that there are low-field components, indicating that ^{57}Fe atoms (lower) move to the Mn layer. Therefore, pure thermodynamic considerations alone cannot completely explain our data. A second model to explain the low-field component (e.g., $B_{hf}\approx 8$ T) and the asymmetry observed at the respective Fe/Mn interfaces has been recently proposed by Uzdin *et al.*[10,24] In their model, they use a ballistic deposition with consequent rising of a fraction of the atoms towards the surface to explain the difference between lower and upper interfaces for Fe/Cr superstructures. The ''diffusion'' process (exchange of atoms) only occurs at the surface *during* the epitaxial growth, without any internal bulk diffusion, i.e., the atoms can only float upwards, but are not allowed to move down due to suppression of internal diffusion. Therefore, the existence of the low-field components suggests actually that ^{57}Fe atoms (lower) float up to the Mn layer during Mn deposition, forming a rich Mn phase with Fe impurities or small Fe clusters. This assumption is also supported by the results reported by Yamada *et al.*,[28] who studied the deposition of Mn on a Fe whisker using scanning-tunneling microscopy (STM). They found that Fe impurities and/or Fe clusters float towards the free Mn surface. In conclusion, from our data we cannot completely exclude either of the two models (thermodynamics and floating of atoms) to interpret the low-field components and the asymmetry effect detected in Fe/Mn interfaces, because they are complementary.

Uzdin *et al.*[24] also published the distribution curves of Fe/Cr superstructures obtained from Mössbauer spectroscopy and from theoretical Hartree-Fock calculations. Different kinds of interface roughness/interdiffusion were modeled using the float model with an Fe interface of 3 ML. In Fig. 12 of Ref. 24, the magnetic-moment distribution curves are very similar for the cases of roughness and roughness+alloying effects, which are almost indistinguishable. Their distribution curves display a main peak at about $2.2\mu_B$ (bulk-Fe value), and several peaks both at higher and lower magnetic-moment values. The hf distribution curves of our Fe/Mn sandwiches have a roughly equivalent shape to the distribu-

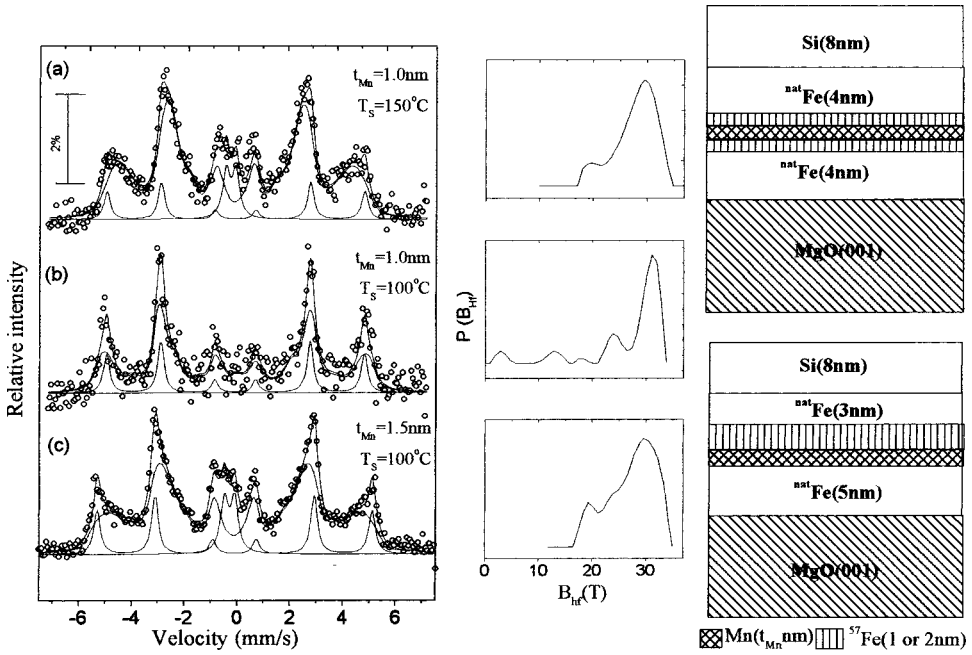

FIG. 5. RT CEM spectra of Fe(5 nm)/Mn(t_{Mn} nm)/Fe(5 nm) trilayers prepared at (a) $T_S=150$ °C and (b) and (c) 100 °C. t_{Mn} is shown in the figure. The points are experimental data, while the full lines correspond to the subspectra and the total fit. On the right side of this figure, the distribution curves associated with the interface component are plotted.

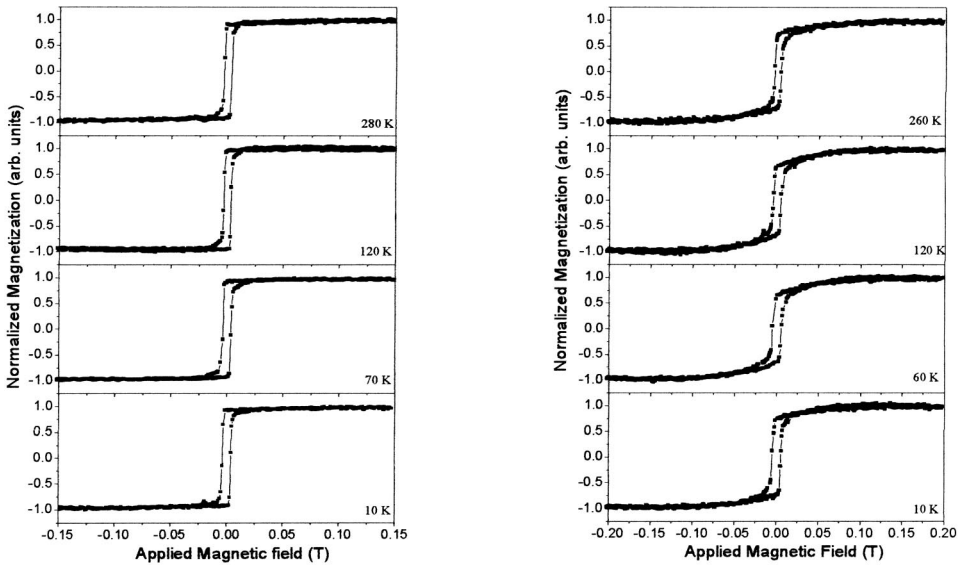

(a) - t_{Mn} = 0.5nm (b) - t_{Mn} = 1.0nm

FIG. 6. (a) and (b) Temperature-dependent in-plane hysteresis loops in the easy direction for Fe(5 nm)/Mn(t_{Mn} nm)/Fe(5 nm) trilayers [t_{Mn}=0.5 (a) and 1.0 nm (b)] prepared at 150 °C.

tion curves of Fe/Cr. However, as opposed to Fe/Cr multilayers, no B_{hf} values larger than the bulk-Fe value have been measured for Fe/Mn sandwiches. Furthermore, the peak at about 20 T in the Fe/Cr system is assigned to Fe atoms interdiffused inside the Cr spacer layers a few atomic layers away from the ideal interface.[24] In case of Fe/Mn, we can also attribute the low-field components to Fe atoms interdiffused inside the Mn spacers, in agreement with the STM results published by Yamada *et al.*[28] Further theoretical modeling is needed to establish the exact configuration of Fe and Mn nearest neighbors, which yields the observed distribution curves for the Fe/Mn sandwiches. Finally, the main peak at about 31 T corresponds to the Fe/Mn ''ideal'' interface with a roughness (or roughness+alloy) as the model proposed by Klinkhammer *et al.*[25] These effects in our films depend basically on the Mn thickness and substrate temperature.

Figure 4 shows the fraction of ''unaffected'' Fe as a function of growth temperature (T_S) for the trilayers. From this figure, it is clear that the ''unaffected'' ^{57}Fe thickness decreases with increasing T_S, corresponding to an increasing thickness of the interface region. Two plausible models may explain this behavior. In a first model, the increase of the interface region is associated with an increase of the atomic interdiffusion with increasing T_S, i.e., enhancement of the formation of an Fe-rich alloy. A second model is related to the increase of roughness at the interface, driven by a tendency for island formation as observed by RHEED. This causes an increase in the number of Fe atoms located in the near vicinity of Mn atoms at the interface. There are two experimental observations that support the second model: (i) the IS values of the main hf distribution component (peak at 31 T) are similar to that of α Fe (this would be expected to be different in the case of the Fe-Mn alloy) and (ii) films of an Fe-Mn alloy would display a paramagnetic spectrum at RT.[29] It is hard to distinguish between roughness or roughness+alloying effects, an argument supported by the calculated magnetic-moment distribution curves obtained for Fe/Cr superstructures (see Ref. 24). Therefore, we conclude that from our results we cannot fully exclude either of the models, although our observations seem to support the second model.

Figure 5 presents the CEM spectra of three trilayers grown at 150 °C [Fig. 5(a)] and 100 °C [Figs. 5(b) and 5(c)], but with different t_{Mn} (1.0 and 1.5 nm), as indicated in the figure. The RT CEM spectrum of the film with t_{Mn} = 1.0 nm, prepared at 100 °C [Fig. 5(b)], displays the same two magnetic components already observed in the films with t_{Mn}=0.5 nm. However, the RT CEM spectrum of the film with t_{Mn}=1.0 nm and prepared at 150 °C [Fig. 5(a)] shows, next to these two magnetic components, a paramagnetic subspectrum with IS=−0.21 mm/s and quadrupole split =0.47 mm/s, which is attributed to the formation of a disordered Fe-Mn alloy.

While it is clear that the alloy formation is related to the film growth temperature, the Mn crystalline phase transition seems to be important as well. For a film growth temperature of 100 °C we do not observe RHEED streaks associated with an α-Mn phase for the trilayer with t_{Mn}=1.0 nm, whereas at 150 °C, an α-Mn pattern appears during the last 0.05 nm of Mn growth. In addition, we prepared a new sample with T_S = 100 °C and t_{Mn}=1.5 nm (α-Mn phase for Mn thickness larger than 1.05 nm), with the ^{57}Fe layer grown on the Mn [see Fig. 5(c)]. In this case, a similar doublet was observed, confirming that this paramagnetic component is related to the Mn crystalline phase transition. Thus, we enunciate that (i) the phase transition itself possibly promotes alloying due to the presence of the defects in the Mn layer[22] and (ii) the α-Mn phase is likely more susceptible to alloying than the bct-Mn phase. This correlation between the Mn phase and alloying/diffusion is a subject for further investigation. We note that the phase transition is accompanied by an increase in the roughness, which also might enhance alloy formation due to an enhancement of the interface reactivity. This increase of roughness was observed both with RHEED and

CEMS. In the latter case, an increasing roughness was concluded from the broader hf distribution curve [Figs. 5(a) and 5(c)] and from the decreasing "unaffected" ^{57}Fe thickness for the trilayers prepared at 150 °C: for $t_{Mn}=0.5$ nm this corresponds to 0.1 nm out of 1 nm ^{57}Fe whereas for $t_{Mn}=1.0$ nm, the "unaffected" ^{57}Fe thickness is about 0.04 nm.

Figures 6(a) and 6(b) display the temperature dependence of the $M(H)$ curves (hysteresis loops) for trilayers prepared at 150 °C with $t_{Mn}=0.5$ and 1.0 nm. The magnetic field is applied in the plane of the film along the ⟨100⟩ Fe easy direction.

From 300 down to 10 K, the hysteresis loops follow the normal trends of conventional magnetic materials, i.e., an increase of M_R, M_S, and H_C with decreasing temperature. In general, the samples with $t_{Mn}=0.5$ nm show no coupling or FM coupling between the Fe layers, since the loops are almost square, i.e., M_R/M_S is close to 1, as shown by Fig. 6(a). Yan *et al.*[5] have reported FM coupling between two Fe layers in Fe/Mn/Fe trilayers for t_{Mn} from 0.08 to 0.5 nm, with a gradual change to a canted FM state above 0.5 nm. For $t_{Mn}=1.0$ nm, they found that the coupling is noncollinear. Filipkowski *et al.*[6] observed noncollinear coupling (near 90° coupling) in FeCo/Mn/FeCo trilayers. This noncollinear behavior is basically attributed to the biquadratic coupling, which is due to the roughness of the magnetic interfaces. In our case, for $t_{Mn}=1.0$ nm and $T_S=150$ °C, we find that $0.5<M_R/M_S<1$ and the saturation field is higher compared to $t_{Mn}=0.5$ nm, which is observed with the magnetic field applied in both the easy and hard Fe directions. The observed magnetic behavior, for the trilayer with $t_{Mn}=1.0$ nm and grown at 150 °C, cannot be simply due to the paramagnetic contribution seen by Mössbauer (doublet) spectroscopy, because the doublet is also present in the trilayer with the Mn thickness of 1.5 nm and prepared at 100 °C, which shows pure FM coupling. Therefore, we can conclude that the trilayer with $t_{Mn}=1.0$ nm and grown at 150 °C has neither a FM nor AFM contribution, but a noncollinear coupling as observed in FeCo/Mn/FeCo.[6] Recently,[30] it has been reported that a noncollinear coupling in Fe/Mn sandwiches with $t_{Mn}>0.5$ nm is enhanced for films prepared at substrate temperatures between 150 °C and 200 °C which looks pretty similar to our results for the film prepared at 150 °C.

IV. SUMMARY AND CONCLUSION

In this work, we studied the structural and magnetic properties of Fe/Mn bi- and trilayers grown by molecular-beam epitaxy. We have shown that the bct-Mn structure is stabilized for a Mn thickness smaller than 1 nm, while 3D Mn features and the α-Mn phase were found for larger Mn thicknesses. RT CEM spectra were analyzed with two magnetic components with in-plane magnetization. A distribution component is associated with Fe atoms close to the interface region, which is affected by spin polarization. Furthermore, low-field components in the hf distribution curves indicate the presence of Fe atoms or/and Fe clusters in the Mn spacers. A second subspectrum is attributed to bulklike Fe atoms far from the interface regions. An Fe-Mn alloy was observed in the case of a Mn thickness larger than 1 nm, where RHEED data indicates enhanced roughness and the presence of the α-Mn phase. Temperature-dependent magnetization loops show that the films exhibit FM or noncollinear magnetic coupling between the Fe layers. No pure AFM coupling between Fe layers was observed in our Fe/Mn films.

ACKNOWLEDGMENTS

The authors thank Dr. Johan Meersschaut for critically reading the manuscript. E. C. Passamani thanks CAPES for a fellowship (Process No. BEX-0673/01-3) and Universidade Federal do Espírito Santo (UFES) which allowed him to work at Katholieke Universiteit Leuven as a visiting scholar. This work was also supported by the Belgian Fund for Scientific Research, Flanders (FWO), the Concerted Action (GOA), and the Inter-University Attraction Pole (Grant No. IUAP P5/1).

[1] P. Grunberg, R. Schreiber, Y. Pang, M. B. Brodsky, and H. Sowers, Phys. Rev. Lett. **57**, 2442 (1986).
[2] D. T. Piece, J. Unguris, R. J. Coletta, and M. D. Stilles, J. Magn. Magn. Mater. **200**, 290 (1999).
[3] A. Fuss, S. Demokritov, P. Grünberg, and W. Zinn, J. Magn. Magn. Mater. **200**, 290 (1992).
[4] Z. Celinski, B. Heinrich, and J. F. Cochran, J. Magn. Magn. Mater. **145**, L1 (1999).
[5] S. S. Yan, R. Schreiber, F. Voges, C. Osthoever, and P. Grunberg, Phys. Rev. B **59**, R11 641 (1999); D. T. Pierce, A. D. Davies, J. A. Stroscio, D. A. Tulchinsky, J. Unguris, and R. J. Celotta, J. Magn. Magn. Mater. **222**, 13 (2000).
[6] M. E. Filipkowski, J. J. Krebs, G. A. Prinz, and C. J. Gutierrez, Phys. Rev. Lett. **75**, 1847 (1995).
[7] P. Bruno, J. Magn. Magn. Mater. **121**, 248 (1993); Phys. Rev. B **52**, 411 (1995).
[8] S. Demokritov, J. Phys. D **31**, 925 (1998); U. Rucker, S. Demokritov, and E. Tsymbal, J. Appl. Phys. **78**, 387 (1995).
[9] J. C. Slonczewski, J. Magn. Magn. Mater. **150**, 13 (1995).
[10] V. M. Uzdin and C. Demangeat, Phys. Rev. B **66**, 092408 (2002).
[11] K. Mibu, N. Hosoito, and T. Shinjo, J. Magn. Magn. Mater. **126**, 343 (1993).
[12] E. C. Passamani, K. Mibu, E. Baggio-Saitovitch, and T. Shinjo, Phys. Rev. B **53**, 6566 (1996).
[13] J. S. Kasper and B. W. Roberts, Phys. Rev. **101**, 537 (1956).
[14] Y. Endoh and Y. Ishikawa, J. Phys. Soc. Jpn. **33**, 1614 (1971).
[15] S. Andrieu, M. Finazzi, Ph. Bauer, H. Fischer, P. Lefevre, A. Traverse, K. Hricovini, G. Krill, and M. Peicuch, Phys. Rev. B **57**, 1985 (1998).
[16] P. Schieffer, C. Krembel, H. C. Hanf, and G. Gewinner, Phys. Rev. B **62**, 2944 (2000).
[17] S. L. Qiu, P. M. Marcus, and Hong Ma, Phys. Rev. B **62**, 3292 (2000); S. L. Qiu and P. M. Marcus, *ibid.* **60**, 14 533 (1999).

[18] R. Q. Wu and A. J. Freeman, Phys. Rev. B **51**, 17 131 (1995).
[19] Ch. Roth, Th. Kleeman, F. U. Hillebrecht, and E. Kisker, Phys. Rev. B **52**, R15 691 (1995).
[20] R. Moons, S. Blässer, J. Dekoster, A. Vantomme, J. De Wachter, and G. Langouche, Thin Solid Films **324**, 129 (1998).
[21] S. K. Kim, Y. Tian, M. Montesano, F. Jona, and P. M. Marcus, Phys. Rev. B **54**, 5081 (1996).
[22] Y. Henry, V. Pierron-Bohnes, P. Vennégues, and K. Ounadjela, J. Appl. Phys. **76**, 2817 (1994).
[23] Ilya L. Grigorov, M. R. Fitzsimmons, I-Liang Siu, and J. C. Walker, Phys. Rev. Lett. **82**, 5309 (1999).
[24] V. M. Uzdin, W. Keune, H. Schorör, and M. Walterfang, Phys. Rev. B **63**, 104407 (2001); V. Uzdin, W. Keune, and M. Walterfang, J. Magn. Magn. Mater. **240**, 504 (2002).
[25] F. Klinkhammer, Ch. Sauer, E. Yu Tsymbal, S. Handschuh, Q. Leng, and W. Zinn, J. Magn. Magn. Mater. **161**, 49 (1996).
[26] B. Kalska, L. Haggstrom, P. Blomquist, and R. Wappling, J. Phys. C **12**, 9247 (2000).
[27] T. Shinjo and W. Keune, J. Magn. Magn. Mater. **200**, 598 (1999).
[28] T. K. Yamada, M. M. J. Bischoff, T. M. Zoguchi, and H. Van Kempen, Surf. Sci. **516**, 179 (2002).
[29] S. K. Xia, E. Baggio-Saitovitch, and C. Larica, Hyperfine Interact. **92**, 1281 (1994).
[30] A. Tulchinsky, J. Unguris, and R. J. Celotta, J. Magn. Magn. Mater. **212**, 91 (2000).